F-14 VSTFE AND RESULTS OF THE CLEANUP FLIGHT TEST PROGRAM

Robert R. Meyer and Bianca M. Trujillo
NASA Ames Research Center
Dryden Flight Research Facility
Edwards, California

Dennis W. Bartlett
NASA Langley Research Center
Hampton, Virginia

VARIABLE-SWEEP TRANSITION FLIGHT EXPERIMENT

Flight transition data applicable to swept wings at high subsonic speeds are needed to make valid assessments of the potential for natural laminar flow or laminar-flow control for transports of various sizes at various cruise speeds. NASA initiated the variable-sweep transition flight experiment (VSTFE) to help establish a boundary-layer transition data base for use in laminar-flow wing design. The carrier vehicle for this experiment is an F-14 aircraft, which has variable-sweep capability. The variable-sweep outer panels of the F-14 aircraft are being modified with natural laminar-flow gloves to provide not only smooth surfaces but also airfoils that can produce a wide range of pressure distributions for which transition location can be determined at various flight conditions and sweep angles. As indicated in figure 1, the current plan is to fly two gloves in the program: glove I, which is a cleanup or smoothing of the basic F-14 wing, and glove II, which has been designed to provide specific pressure distributions at Mach 0.7 (ref. 1). A glove III was also designed for Mach 0.8 (ref. 2) but will probably not be flown (NASA expects to lose custody of the F-14 aircraft before glove III can be flown). The majority of the glove I flight tests have been completed, and glove II flight tests are planned for spring and summer of 1987. This paper briefly describes the VSTFE program and presents some preliminary glove I flight results.

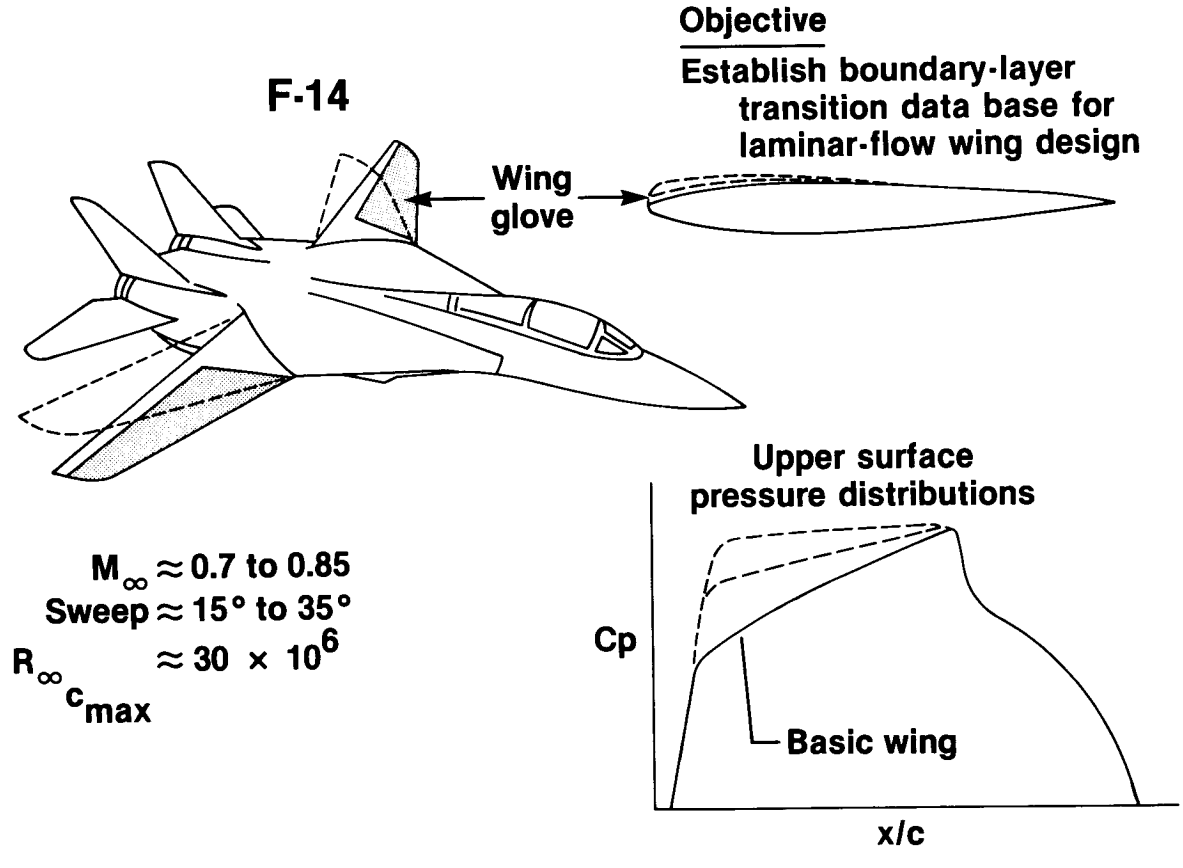

Figure 1

F-111/TACT NLF GLOVE

The catalyst for the present VSTFE program was the encouraging results from an earlier NASA flight test program, the F-111/TACT natural laminar flow (NLF) experiment (refs. 3 and 4). The NLF flight test program provided the first definitive flight results on the effects of wing sweep on boundary-layer transition. A complete supercritical NLF airfoil was "gloved" around the right wing panel of the F-111/TACT aircraft (fig. 2). This glove, made of foam and fiberglass, had a span of approximately 6 ft and a chord of 10 ft. Although the glove was designed for a 10° sweep, data were obtained at sweep angles as high as 26°. At sweep angles near 10°, transition occurred at about 55-percent chord (transition Reynolds numbers of about 15×10^6), but for a 26° sweep, transition occurred in the 10- to 20-percent chord range. In addition to providing transition data, this program helped develop the construction techniques for making large contour modifications to metal wings from foam and fiberglass (ref. 5).

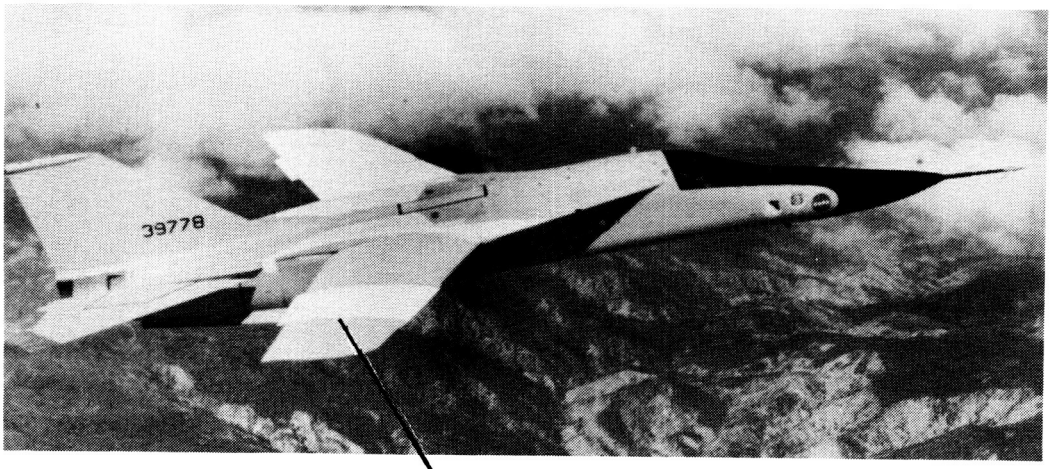

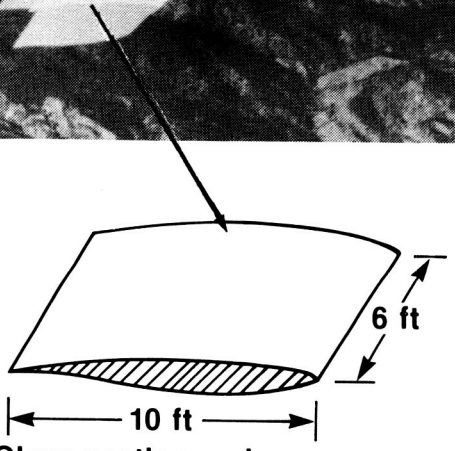

Glove section and span

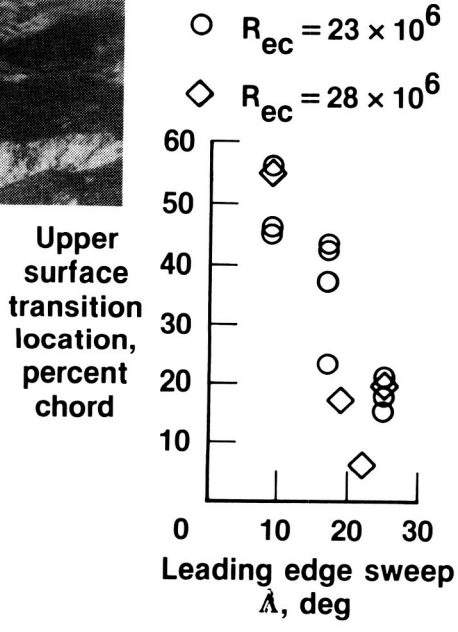

Figure 2

F-111/TACT NLF ENHANCEMENT OF BOUNDARY-LAYER STABILITY PREDICTION METHODS

In the past, semiempirical transition prediction methods have been enhanced by correlating boundary-layer stability theory with experimentally obtained transition data from the F-111/TACT NLF flight test program (refs. 3 and 6). The computational approaches generally utilize linear noninteracting boundary-layer stability analysis conducted for the Tollmien-Schlichting (T-S) and cross-flow (C-F) disturbances. The natural log of the most amplified disturbance growth, or N factor, of each type is then correlated to empirically derived limits to assess the likelihood of transition.

In one approach, (refs. 3, 6, and 7), analytically derived T-S N factors and C-F N factors for stationary disturbances are correlated with experimentally derived transiton locations obtained from F-111/TACT NLF results. The resultant S-shaped (cross-hatched) region in figure 3 indicates the combined T-S and C-F N-factor values for which transition is determined to occur. Consequently, this method predicts that transition will occur when any combination of T-S and C-F N factors reaches the values defined by the S-shaped region in figure 3.

Prior to the F-111/TACT NLF flight experiment, it was suggested (ref. 8) that a linear coupling existed between T-S and C-F disturbances. The relationship between the linear coupling and the S-shaped F-111/TACT NLF criteria indicates that the adverse effect of wing sweep is not as severe at higher sweep angles as had been originally assumed.

Another approach (ref. 9) also uses linear noninteracting boundary-layer stability theory. However, the calculations are conducted for stationary and nonstationary C-F and T-S disturbances, and transition is presumed to occur when growth of either disturbance has reached a certain N factor. Some previous correlations (refs. 10 and 11) with experimental data indicate that the value of N at transition should be in the range of 9 to 12 if all variables are taken into account.

The F-111/TACT NLF experiment was originally designed for a leading-edge sweep of 10°. The data were obtained for only one airfoil shape, and data defining the lower right-hand portion of the S-shaped curve were limited. More follow-on variable-sweep experimental data were needed for different airfoil shapes. Unfortunately, the F-111 aircraft used for the previous experiment was committed to another program and was unavailable for laminar-flow experiments. Consequently, another variable-sweep aircraft was sought.

Figure 3

F-111/TACT NLF ENHANCEMENT OF BOUNDARY-LAYER STABILITY PREDICTION METHODS

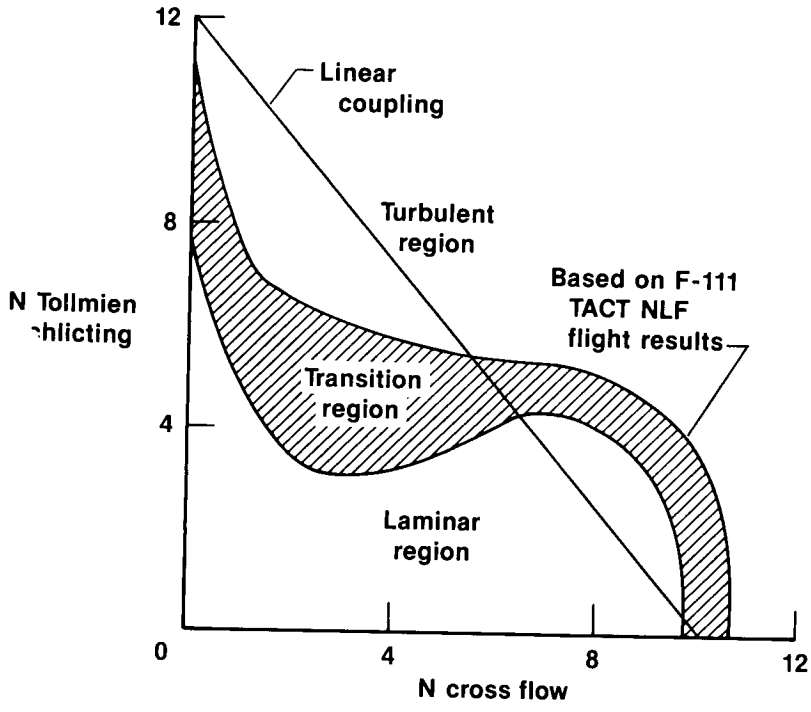

Problem

- F-111/TACT NLF originally designed for 10° leading-edge sweep but most data obtained at 20° and 25° leading-edge sweep
- Data on lower portion of curve limited
- Different airfoil shapes needed to be evaluated

F-14 VSTFE AIRCRAFT DESCRIPTION

An F-14 aircraft was chosen as the carrier vehicle for the VSTFE program, primarily because of its variable-sweep capability, Mach and Reynolds number capability, availability, and favorable wing pressure distribution (ref. 12). A laminar-flow glove (glove I) was installed on the upper surface of the left wing panel (fig. 4). The standard radome on the aircraft was replaced with a flight test radome that incorporated a flight-test-quality pitot-static probe equipped with alpha and beta vanes (ref. 13). The cockpit of the aircraft was equipped with a special display that allowed for trajectory guidance signals to be uplinked and displayed to the pilot in real time (ref. 14). With the laminar-flow glove installed, the wing sweep capability was restricted to a range of 20° to 35° leading-edge sweep, and the flaps and slats were locked in an up position. The basic aircraft glove vanes were disabled for these flight tests. A 15° leading-edge sweep was simulated by sideslipping the aircraft 5° at 20° sweep, resulting in an equivalent sweep of 15°.

F-14A provides

- **Variable sweep**
- **Mach/Reynolds number envelope**
- **Favorable wing pressure distribution**

"Cleanup" glove (Glove I) installed on left wing upper surface leading edge

Sweep range

- **20° to 35°**
- **Simulate 15° with β = 5°**

Slats and flaps locked in up position

Figure 4

GLOVE I CONSTRUCTION

Glove I was installed to provide an equivalent "sailplane finish" on the existing F-14 wing. It was determined that the extra thickness of the glove would have only a minor influence on the pressure distribution shape or thickness/chord ratio. The glove wraps around the wing leading edge (disabling leading-edge slats), extends aft to just forward of the spoiler hinge line (approximately 60-percent chord), and covers most of the span (fig. 5). The glove was constructed by applying a constant-thickness foam and fiberglass surface over the existing wing skin (a method similar to that described in ref. 5). The glove was approximately 0.65 in thick, initially consisting of one layer of fiberglass, 0.5 in of polyurethane foam, six layers of fiberglass, and a finish of polyester body filler and paint. During the flight envelope verification flights, small surface cracks developed in the glove. These cracks probably resulted from lateral stick rap maneuvers performed for structural excitation during the flutter clearance phase of the flight test. To repair these cracks, one additional layer of fiberglass was applied over the surface of the glove. The final glove incorporated this one additional layer of fiberglass and a finish of polyester body filler and paint.

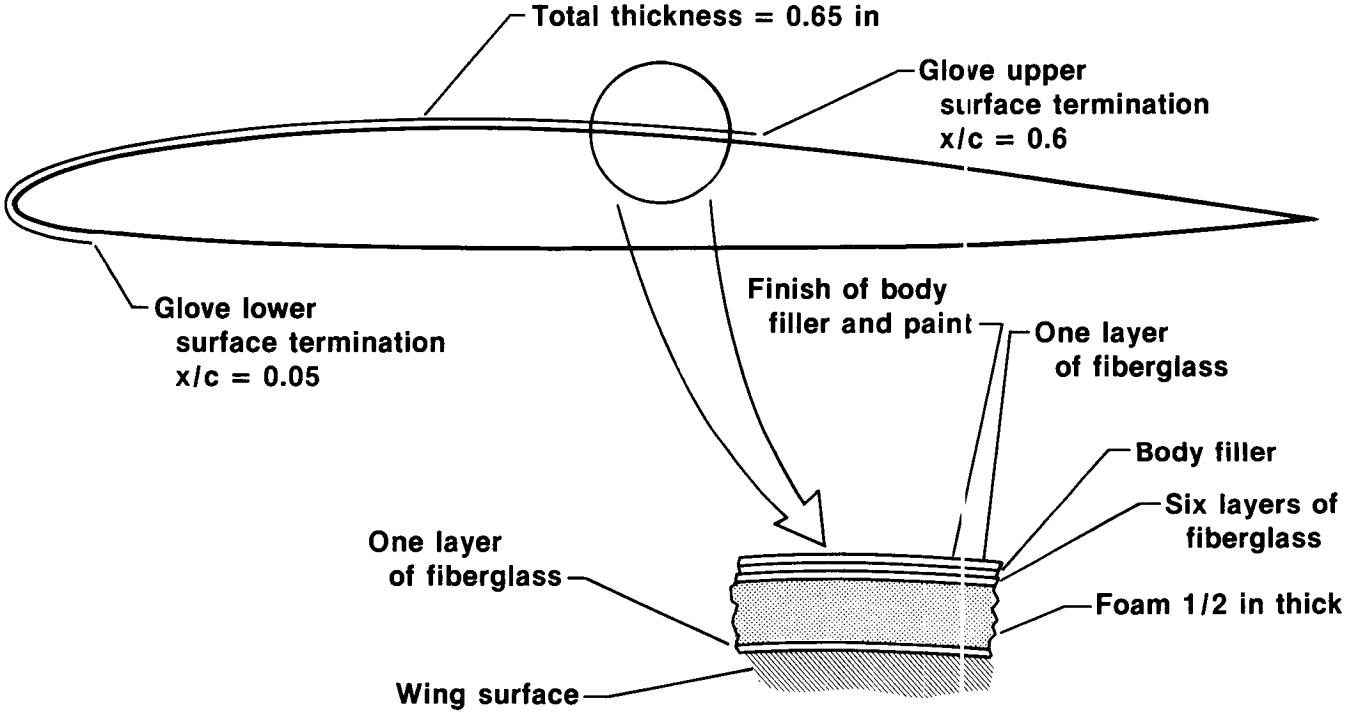

Figure 5

GLOVE I WAVINESS MEASUREMENTS

Figure 6 presents surface curvature measurements for three wing stations on glove I. These measurements were taken with the wing unloaded (zero load) and with the wing jacked from the lower surface to simulate a 1-g loaded condition, which was the condition for most of the flight tests. The measurements were obtained with a mechanical deflection dial gauge having support feet 2-in apart. The dial gauge was equipped with a wheel from which the distance along the glove surface could be determined. The outputs from both the dial gauge and the wheel were automatically plotted when the unit was manually moved across the surface. Because of the long chord lengths involved, two people were required to make the measurements; this resulted in an apparent roughness at the gauge "handoff" locations. In general, the glove is not as smooth in the simulated 1-g loaded condition as in the unloaded condition; however, even for this case, the wave amplitudes are within 0.002 in/in, the criterion specified for glove construction.

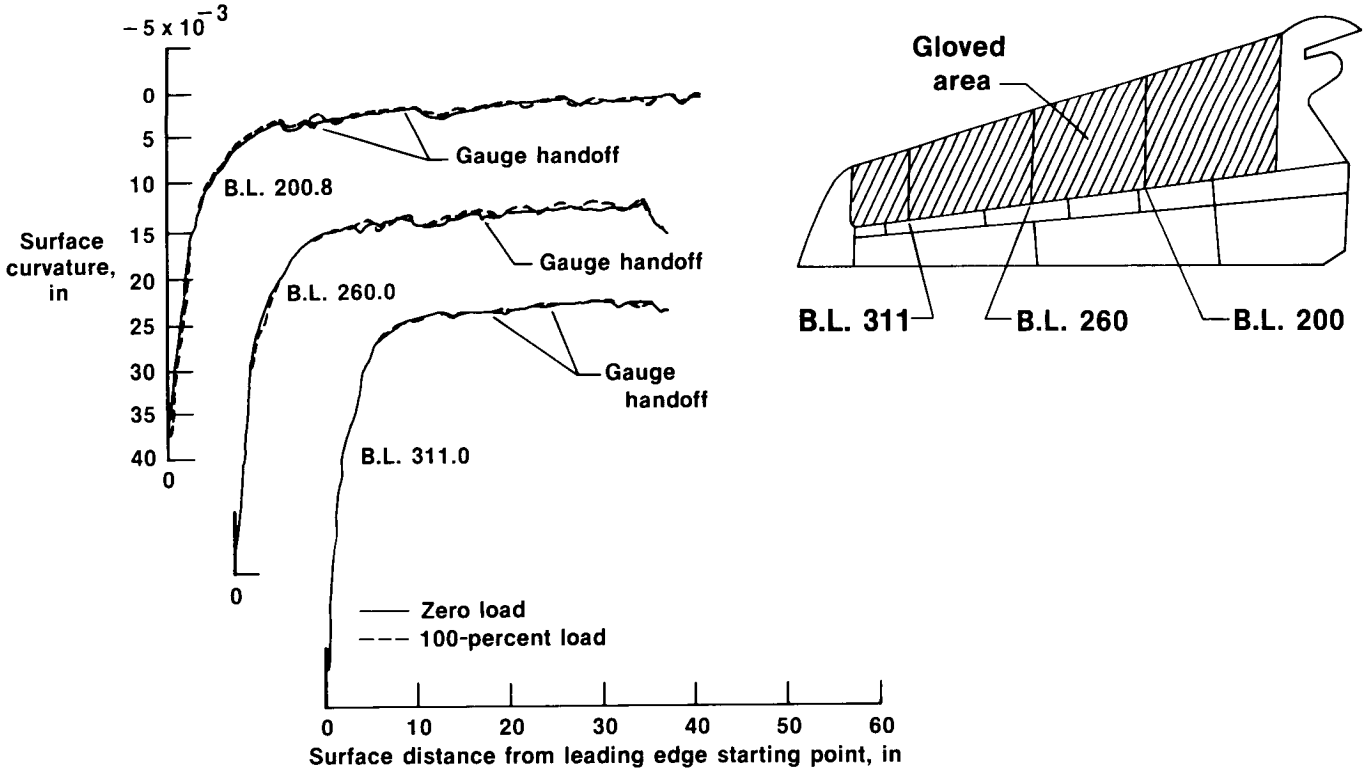

Figure 6

GLOVE I PLANFORM AND INSTRUMENTATION

The glove was instrumented as shown in figure 7. All signals from the instruments were recorded onboard the aircraft, and most were downlinked to a ground station for real-time display and recording. Data from the pitot tubes, dynamic transducers, strain gauges, skin temperature gauges, or accelerometers are not discussed in this paper. The three rows of surface pressure orifices were located at butt line stations of 200, 260, and 320. The orifices were drilled through the glove surface into small cavities built into the glove. Pressure lines were routed internally through the glove to lower surface wing compartments, where the transducers were located. Each boundary-layer rake consisted of 20 pitot tubes distributed along a 4-in strut, which was slanted 30° from the surface of the glove. Pressure lines were routed internally through the glove to the lower surface wing compartments.

The locations of the five hot-film gauges varied from flight to flight. Each was oriented streamwise to the flow for a wing sweep of 20°. To alleviate interference between the hot-film gauges, they were placed along a line oriented 30° to each orifice row (30° to the streamline at 20° sweep). Electrical wires from the hot-film gauges were routed externally along the glove surface to wing compartments. Additionally, the output signals were monitored in real time in the F-14 cockpit using an intercom audio system. This system allowed the pilot to affect transition location through the modification of either flight path or wing sweep.

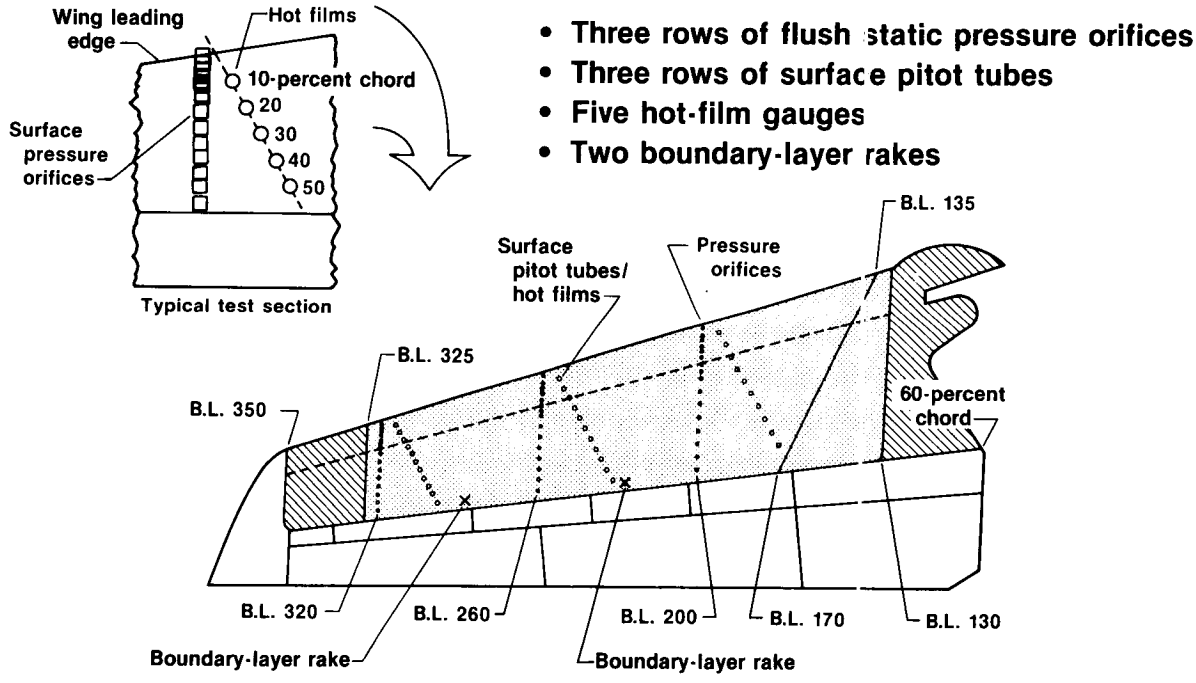

Figure 7

FLIGHT TEST ENVELOPE

Initial flights were designed to clear an operating envelope that was free from flutter and to obtain an airspeed calibration. Flutter data were obtained during stable Mach number and altitude conditions using control raps and natural turbulence for vehicle excitation. Airspeed calibration data were obtained from an acceleration-deceleration method and tower flybys (refs. 15 and 16). Maximum airspeed limit on the aircraft with the glove installed was 450 knots indicated airspeed or Mach 0.9, whichever occurred first (fig. 8). Reynolds number could be varied from approximately 1.0×10^6 ft^{-1} to 4.0×10^6 ft^{-1}, or a minimum and maximum chord Reynolds number of 5.0×10^6 to 34.0×10^6, respectively.

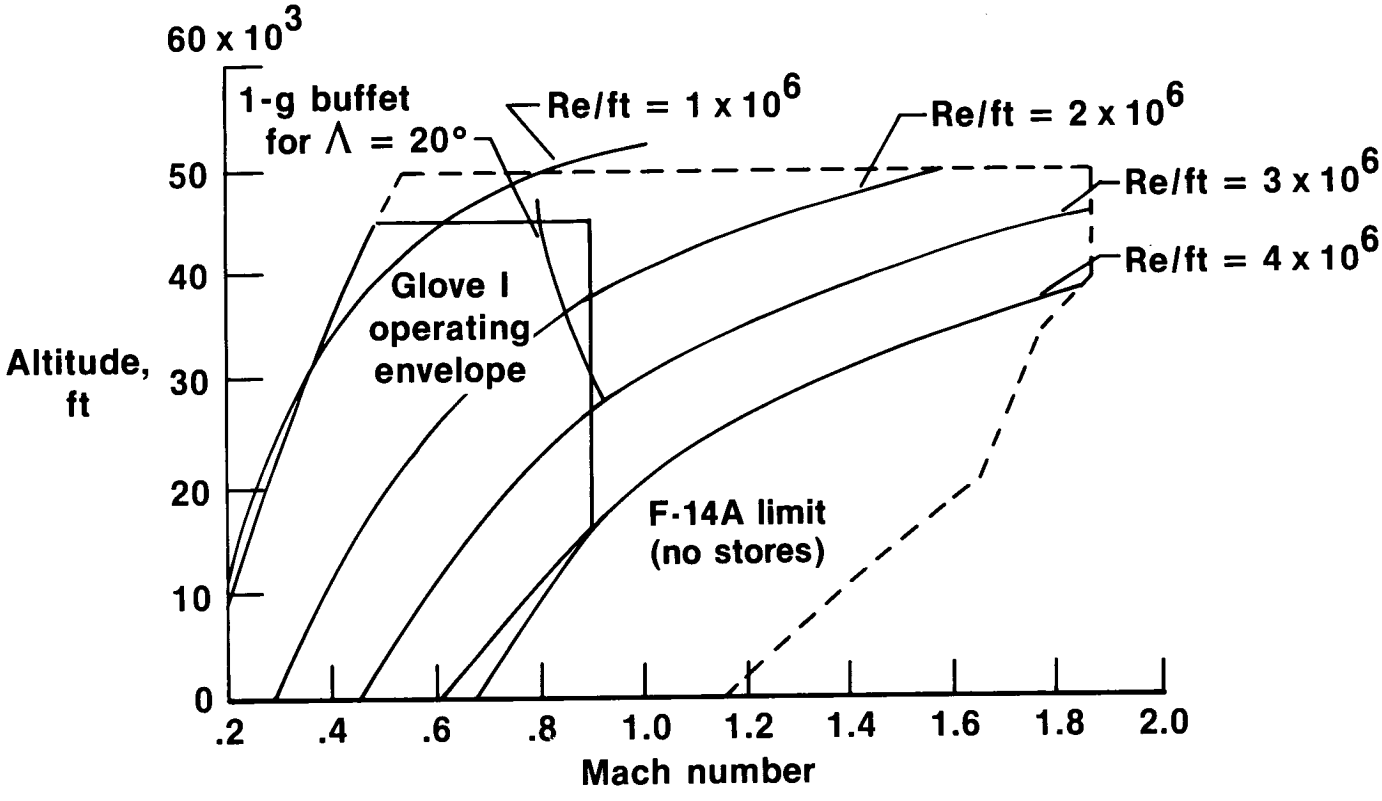

Figure 8

TYPICAL FLIGHT TEST MANEUVERS AND
UPPER SURFACE PRESSURE DISTRIBUTIONS

Laminar-flow data flights were conducted within the cleared envelope. First, coarse-resolution survey flights were conducted, followed by more detailed surveys to establish transition location as a function of wing sweep, angle of attack, Mach number, and Reynolds number (altitude). Maneuvers performed during the coarse-resolution survey flights consisted primarily of trim points and level turns. The level turns were used to obtain data at greater than 1-g trim angle of attack, particularly at low altitudes (high dynamic pressure). Figure 9 presents typical butt line (B.L.) 260 (middle test section) pressure distributions at trim angle of attack and Mach numbers of 0.7 and 0.8. The most notable characteristic is the change in the leading-edge pressure gradient $\Delta CP/\Delta(x/c)$ and pressure distribution shape with Mach number. At Mach 0.7 the gradient is less steep and becomes mildly adverse near 30-percent chord (x/c = 0.3), whereas at Mach 0.8 the favorable pressure gradient is much steeper and extends to 50-percent chord (x/c = 0.5), where a shock wave occurs. One undesirable characteristic of the pressure distribution at Mach 0.7 is the formation of an adverse pressure gradient near the leading edge with increasing angle of attack. This adverse gradient precludes laminar flow aft of the leading edge region. However, it was possible to alleviate these undesirable characteristics by performing a pushover maneuver, as described in the discussion of figure 10.

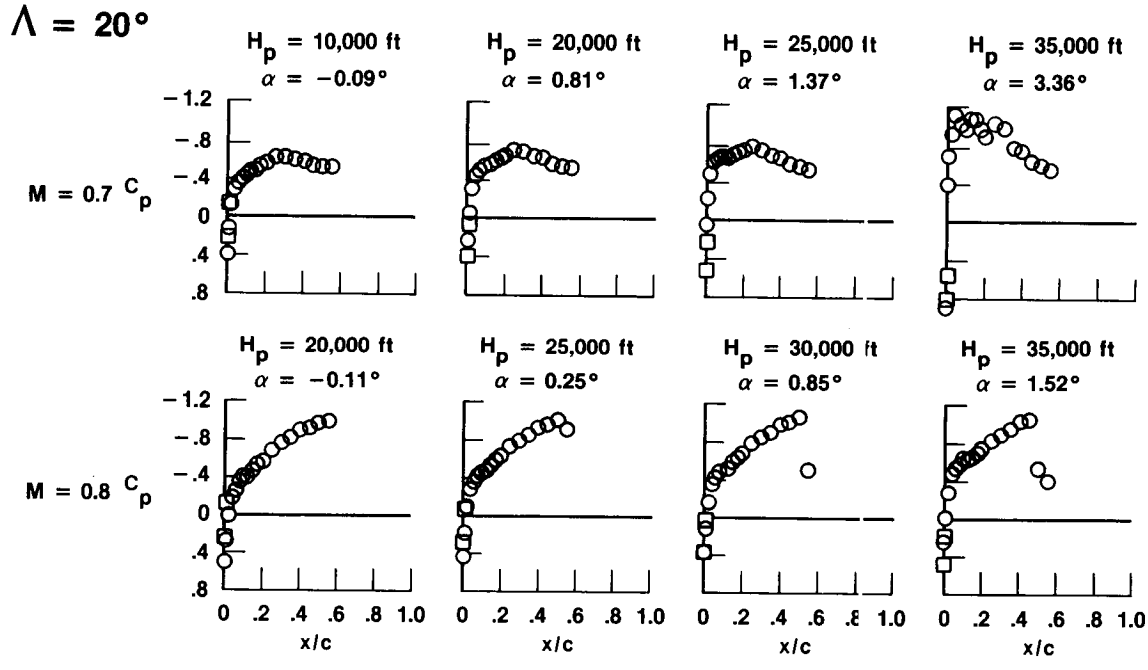

Figure 9

PUSHOVER MANEUVER

At certain combinations of Mach number, wing sweep, and altitude, it was necessary to perform a pushover maneuver to obtain a suitable pressure distribution on the glove. A smooth pushover maneuver that fulfilled these requirements was developed. Figure 10 shows typical time histories of angle of attack, altitude, and Mach number during such a pushover maneuver. For this example, trim angle of attack was approximately 2.0°, and desired angle of attack was 0.5°. The maneuver was started with a pullup at a flight condition slightly below the desired altitude and slightly above the test Mach number. The pull-up was followed by a pushover to the desired angle of attack, and conditions were maintained for approximately 10 sec before a recovery pullout was initiated. The ability to develop and perform this maneuver was attributed primarily to the real-time cockpit display.

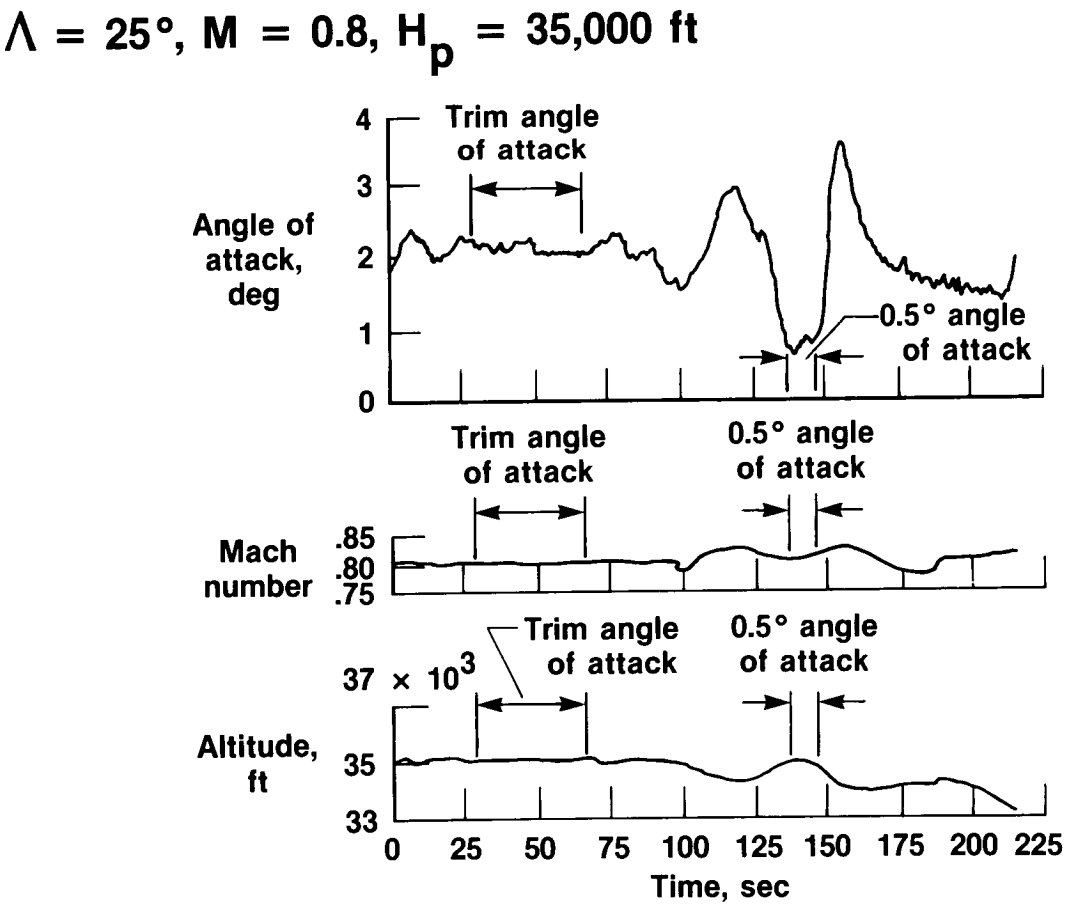

Figure 10

HOT-FILM ANEMOMETER AND PRESSURE DISTRIBUTION RESULTS

Hot-film anemometer interpretation was the primary method for determing transition location. Typically the hot-film gauges were located at 10-, 20-, 30-, 40-, and 50-percent chord on a particular test section. Outputs were plotted on a strip chart as functions of time. Two types of time histories were obtained: One consisted of low-frequency response plots displayed in real time in the ground station. The other consisted of high-frequency response plots that were made postflight. Signals originating in areas of laminar flow were of lower amplitude or quieter than those originating in areas of turbulent flow (fig. 11). Additional indicators were spikes in the output signal; spikes in a direction of positive voltage indicated a mostly laminar signal with occasional turbulent bursts, and spikes in a direction of negative voltage indicated a mostly turbulent signal with occasional laminar bursts. Maximum occurrence of these spikes was at peak transition, or the region where the flow is most unstable. The real-time ground station plots were generally acceptable for determining transition location; however, in some cases the high-frequency response plots were needed for clarification.

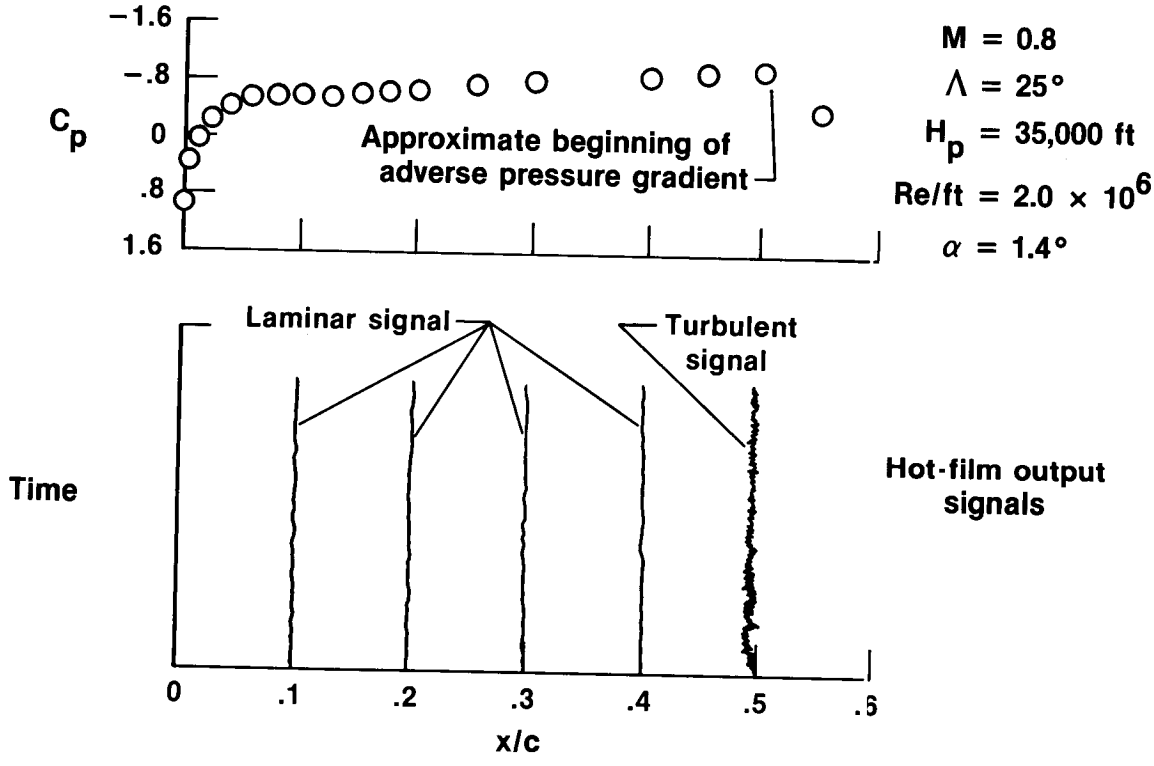

Figure 11

DETERMINING TRANSITION LOCATION
FROM BOUNDARY-LAYER MEARUREMENTS

Boundary-layer profile measurements were used as a secondary source for determining approximate transition location and as a source for determining skin-friction-related parameters. Transition location was determined by measuring the boundary-layer thickness δ as a function of angle of attack for a given sweep angle, Mach number, and altitude at various forced transition locations. Comparing the clean wing results (natural transition) with the calibration data (where transition was forced with grit strips using the method described in ref. 17) provided an indication of the extent of laminar flow achieved on the test section (fig. 12).

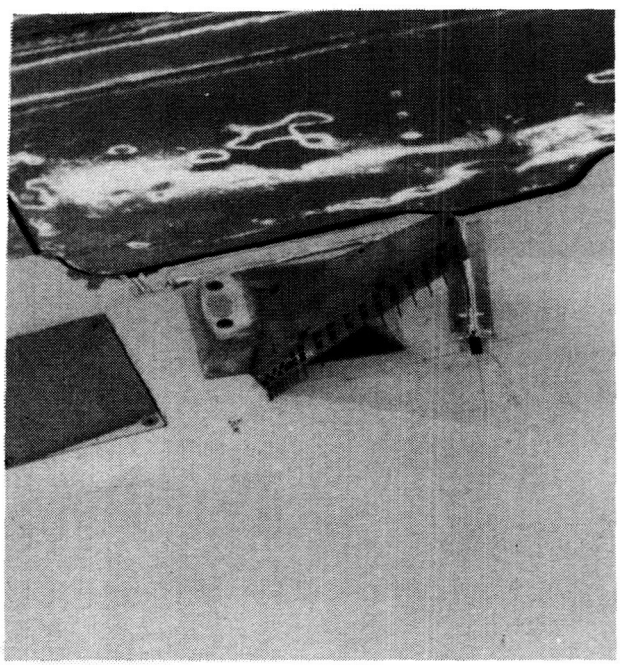

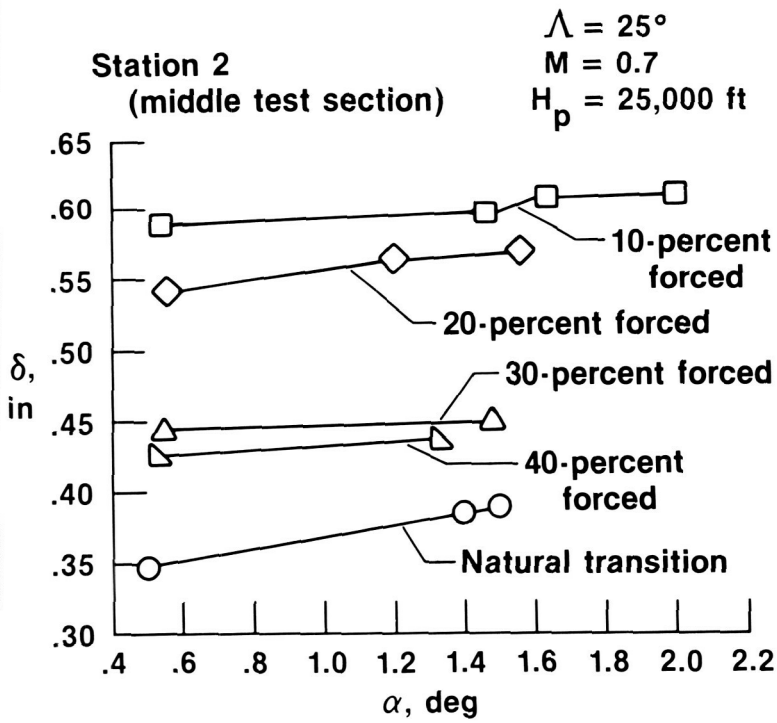

Figure 12

FLOW VISUALIZATION RESULTS

A flow visualization technique utilizing liquid crystals provided encouraging results. The technique was similar to that described in reference 18; a liquid crystal chemical in an oil base was applied with a brush to the wing glove surface prior to takeoff. However, the chemicals used in this case were primarily sensitive to shear. These chemicals provided results over a wider altitude and speed range than the temperature-sensitive chemicals used in reference 18.

For the flow visualization flights, the middle test section (station 2) was refinished with black paint to provide contrast with the liquid crystals. Photographs of the liquid crystal patterns were taken from a chase aircraft flying in close formation. Figure 13 presents a photograph of the liquid crystal patterns on the middle test section along with pressure distribution and hot-film anemometer traces for Mach 0.7, an altitude of 20,000 ft, and an equivalent wing sweep of 15°. The contrast change appears in the photo at 35-percent chord, indicating an abrupt change from laminar to turbulent flow. A wedge-shaped pattern emanates from the leading-edge region near the outboard portion of the test section. The wedge is a small region of turbulent flow believed to be caused by a surface discontinuity, such as dirt or an insect impact. The wedge is located forward of the 30-percent chord hot-film gauge with the edge of the wedge near the 20-percent chord hot-film gauge. The photographic observations are consistent with information from the pressure distribution and hot-film anemometer traces. The pressure distribution shows an adverse pressure gradient beginning at about 30-percent chord, indicating that the laminar boundary layer exists approximately 5-percent chord beyond the beginning of the adverse gradient. The hot-film anemometer traces indicate a laminar signal at 10-percent chord, an intermittent (but mostly laminar) signal at 20- and 30-percent chord, and a turbulent signal at 40- and 50-percent chord. The intermittent signal probably results from the turbulent wedge.

FLOW VISUALIZATION RESULTS

$\Lambda = 20°$, $\Lambda_{equiv} = 15°$, $\beta = -5°$, $M = 0.7$, $H_p = 20{,}000$ ft

$\alpha = 0.7°$

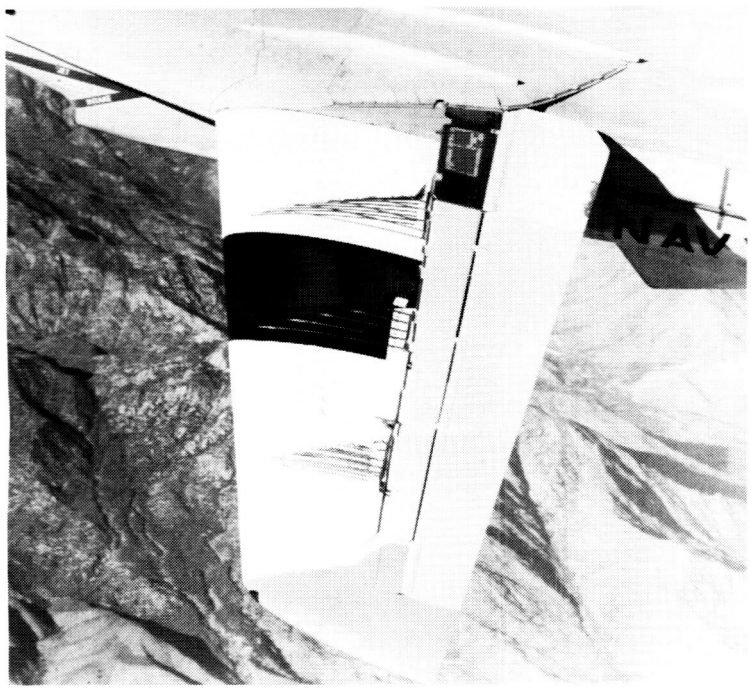

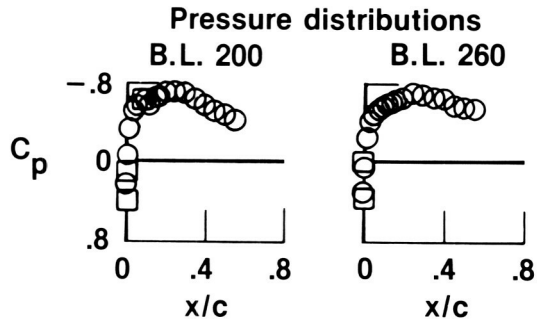

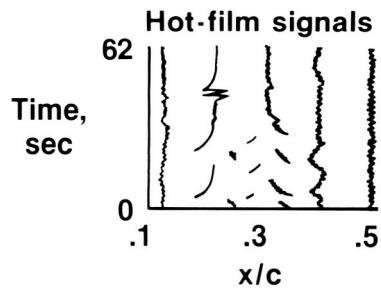

Figure 13

FLOW VISUALIZATION RESULTS

Figure 14 presents another photograph of the liquid crystal patterns on the middle test section with the corresponding pressure distribution and hot-film anemometer trace for Mach 0.8, an altitude of 25,000 ft, and a wing sweep of 20°. The contrast change in this photograph occurs in a sawtooth pattern between 10- and 20-percent chord. This indicates spanwise variation from laminar to turbulent flow. The pressure distribution shows a favorable pressure gradient existing to about 50-percent chord, indicating that the laminar boundary layer undergoes transition forward of the adverse gradient, which is the likely result of cross flow. The hot-film anemometer traces indicate a laminar signal at 10-percent chord and turbulent signals at 20-, 30-, 40-, and 50-percent chord. The traces are consistent with the liquid crystal pattern.

$\Lambda = 20°$, $M = 0.8$, $H_p = 25{,}000$ ft, $\alpha = 0.2°$

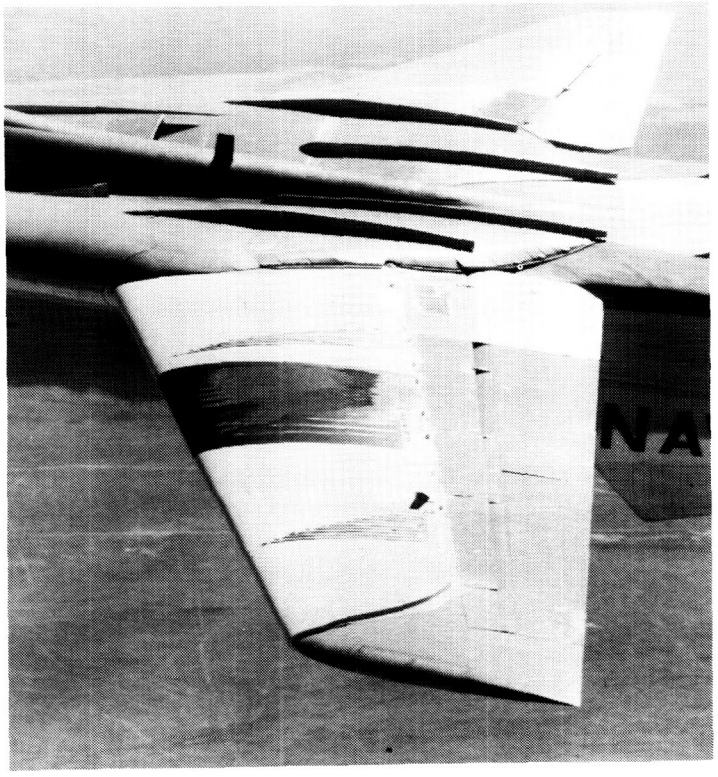

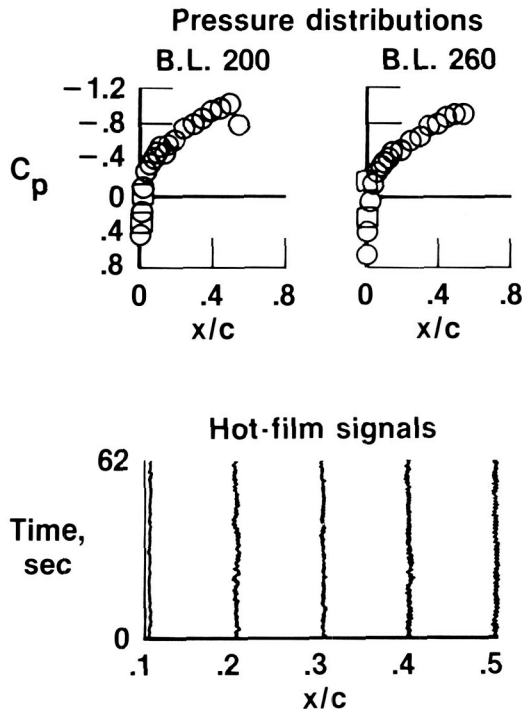

Figure 14

TYPICAL DETERMINATION OF TRANSITION LOCATION

Using hot-film anemometer and boundary-layer measurements, transition location was plotted as a function of angle of attack. Figure 15 shows a typical transition location plot at Mach 0.7, an altitude of 35,000 ft, and a wing sweep of 20° for the three test sections of the glove. The chord location of the beginning of the adverse gradient, shown as a dashed line in the figure, was obtained from analysis of data such as those presented in figure 9. For the middle and outboard test sections (stations 2 and 3), transition occurred at 40- to 50-percent chord (x/c = 0.4 to 0.5) for angles of attack below about 1.75°. The scatter in the data at station 2 for the more aft transition location (x/c = 0.4) was typically ±5-percent chord. It is interesting to note that transition occurred approximately 10-percent chord aft of the adverse pressure gradient on the middle and outboard test sections. The most aft transition on the inboard section occurred at slightly greater than 30-percent chord (x/c = 0.3). On all three test sections the data indicate a forward movement of transition location with increasing angle of attack. This is attributed to the previously mentioned localized adverse pressure gradient that occurs with increasing angle of attack. For example, at the middle test section (station 2), for this Mach number and wing sweep, a strong adverse pressure gradient formed at about 20-percent chord for 1.75° angle of attack, moving the transition location to about the 20-percent chord (x/c = 0.2) location.

It should be noted that the Mach 0.8 pressure distribution, as shown in figure 9, provided a favorable pressure gradient extending to about 50-percent chord (x/c = 0.5), where a shock wave occurred. The position and steepness of the adverse leading-edge gradient could be controlled in flight with Mach number, within the range of the Mach 0.7 and 0.8 pressure distributions shown in figure 9.

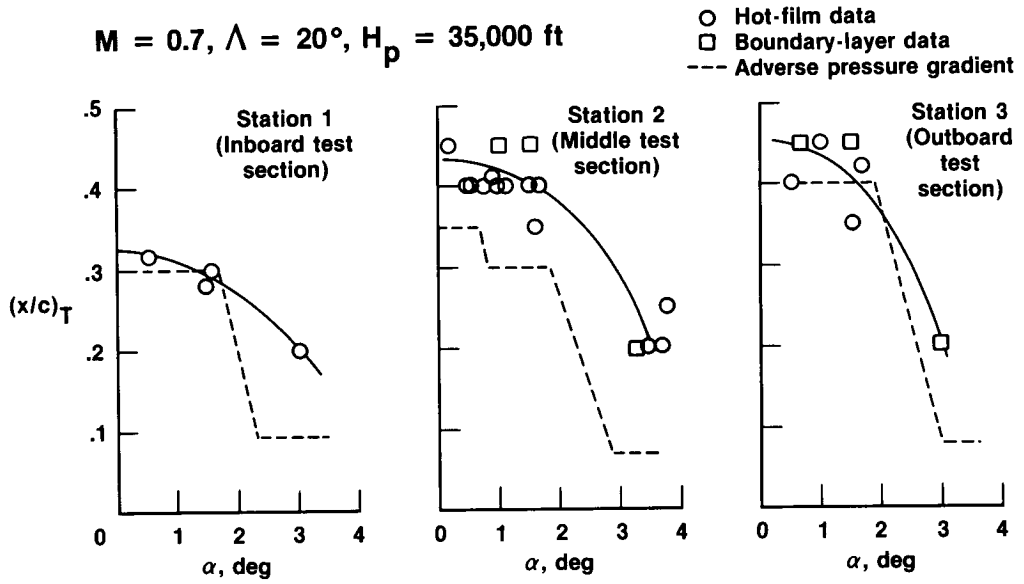

Figure 15

EFFECT OF WING SWEEP ON
TRANSITION LOCATION AT MACH 0.7

Figure 16 presents the most aft or optimum* transition location as a function of wing sweep for two altitudes at Mach 0.7. The data were obtained from results typical of those presented in figure 15 at the angle of attack at which the most aft transition occurred. For example, at 35,000 ft for the middle and outboard test sections (stations 2 and 3), the transition location varied from 45-percent chord at 20° wing sweep, to 35-percent chord at 35° wing sweep. For the inboard test section (station 1), transition location varied from 32-percent chord at 20° wing sweep to 10-percent chord at 35° wing sweep. The more forward transition location on the inboard test section is attributed to a less favorable pressure distribution and increased chord Reynolds number.

*Optimum refers to the most aft transition location observed from hot-film anemometer and boundary-layer measurements at these condtions (Mach number and wing sweep), but not necessarily the most aft obtained at other conditions (other Mach numbers and wing sweeps).

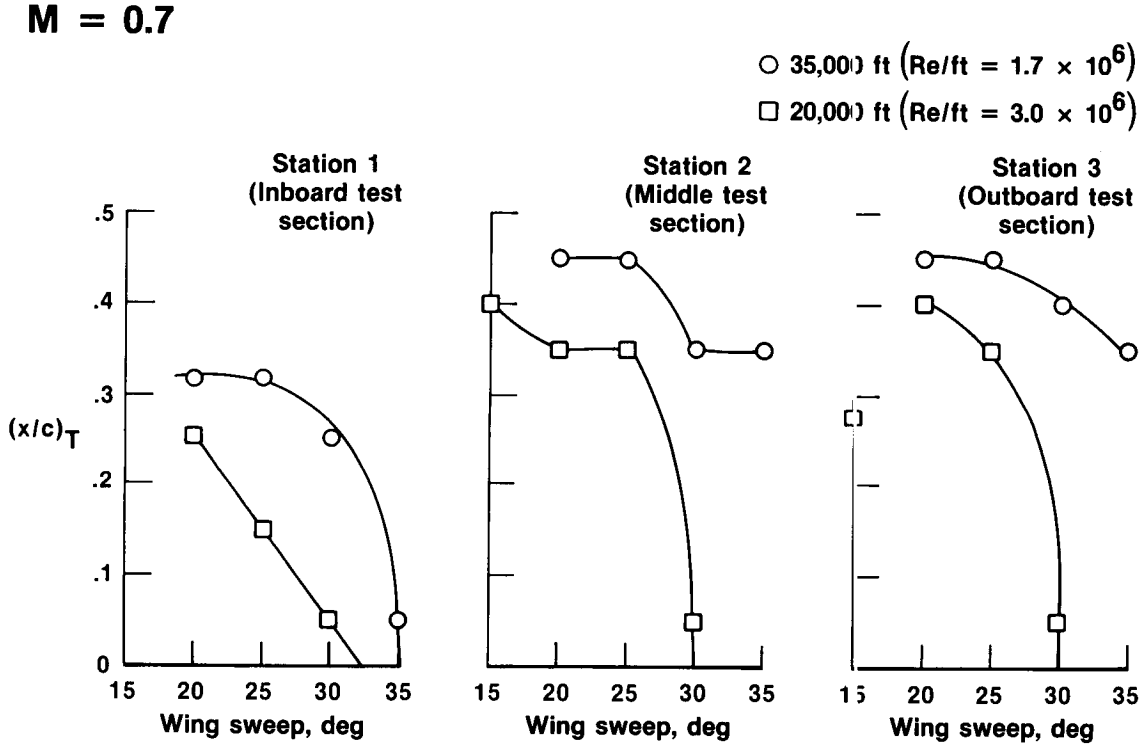

Figure 16

EFFECT OF WING SWEEP ON
TRANSITION LOCATION AT MACH 0.8

Figure 17 presents optimum transition location as a function of wing sweep for two altitudes at Mach 0.8. The results are generally similar to those presented in figure 16, with the exception that wing sweep has a more pronounced effect on transition location. For example, on the middle test section (station 2) transition is aft of 50-percent chord at 20° wing sweep and moves forward to 10-percent chord at 35° wing sweep. The increased effect of sweep is attributed to the steeper leading-edge pressure gradient at Mach 0.8, which increases the likelihood of cross-flow-type disturbances.

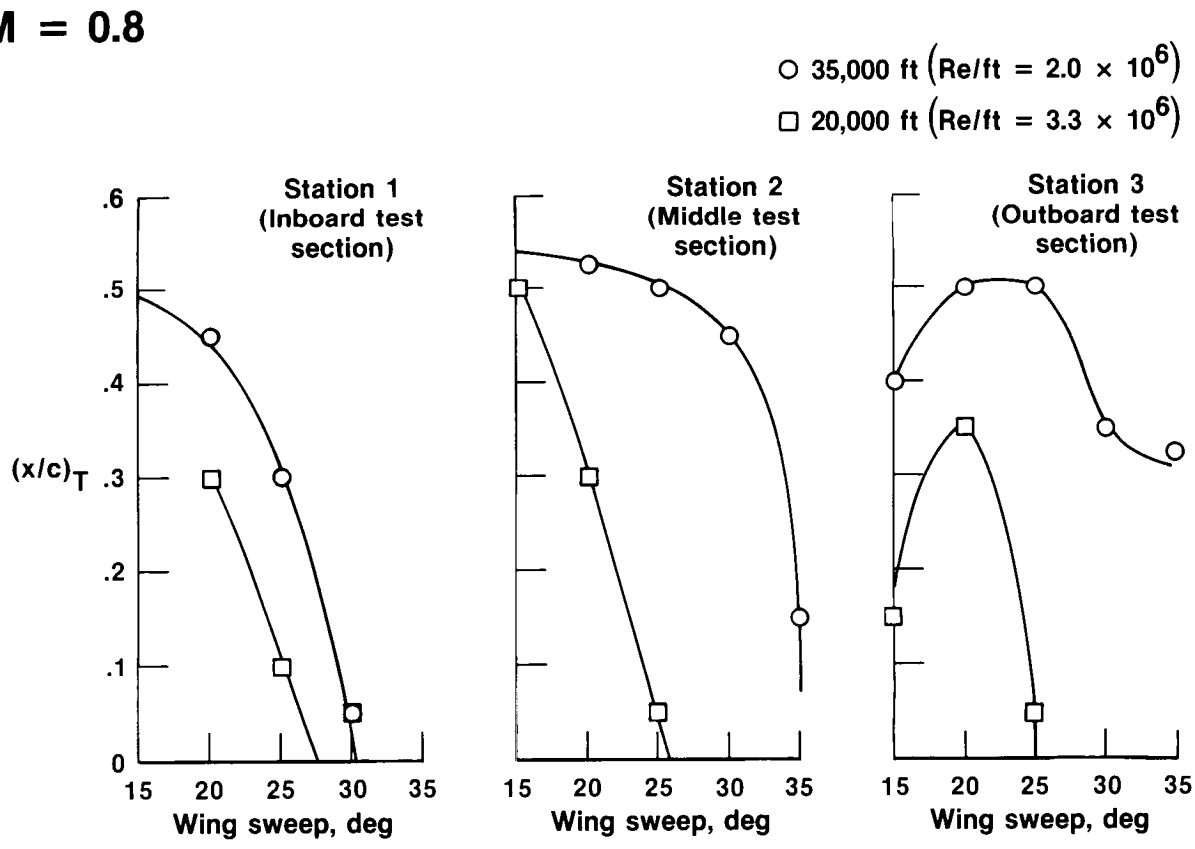

Figure 17

TRANSITION REYNOLDS NUMBER
AS A FUNCTION OF WING SWEEP

Figure 18 presents transition Reynolds number as a function of wing sweep at Mach 0.7 and 0.8. Maximum transition Reynolds number of approximately 13×10^6 occurs on the middle test section at a wing sweep of 15° for both Mach 0.7 and 0.8 data. It is interesting to note that transition Reynolds number decreases almost linearly with wing sweep at Mach 0.8. This is attributed to the highly favorable pressure gradient at this Mach number. The extent of this highly favorable pressure gradient (fig. 9) and the fact that transition occurred forward of the adverse pressure gradient are probably due to Reynolds-number-related phenomena, such as cross-flow disturbances. For the Mach 0.7 data, transition Reynolds number decreases in a nonlinear fashion with wing sweep. This is attributed to the less favorable pressure gradient at Mach 0.7 and to the more forward location of the adverse gradient, conditions that allow transition to occur sometimes because of the adverse gradient and sometimes because of Reynolds-number-related phenomena in the favorable gradient, such as cross-flow disturbances.

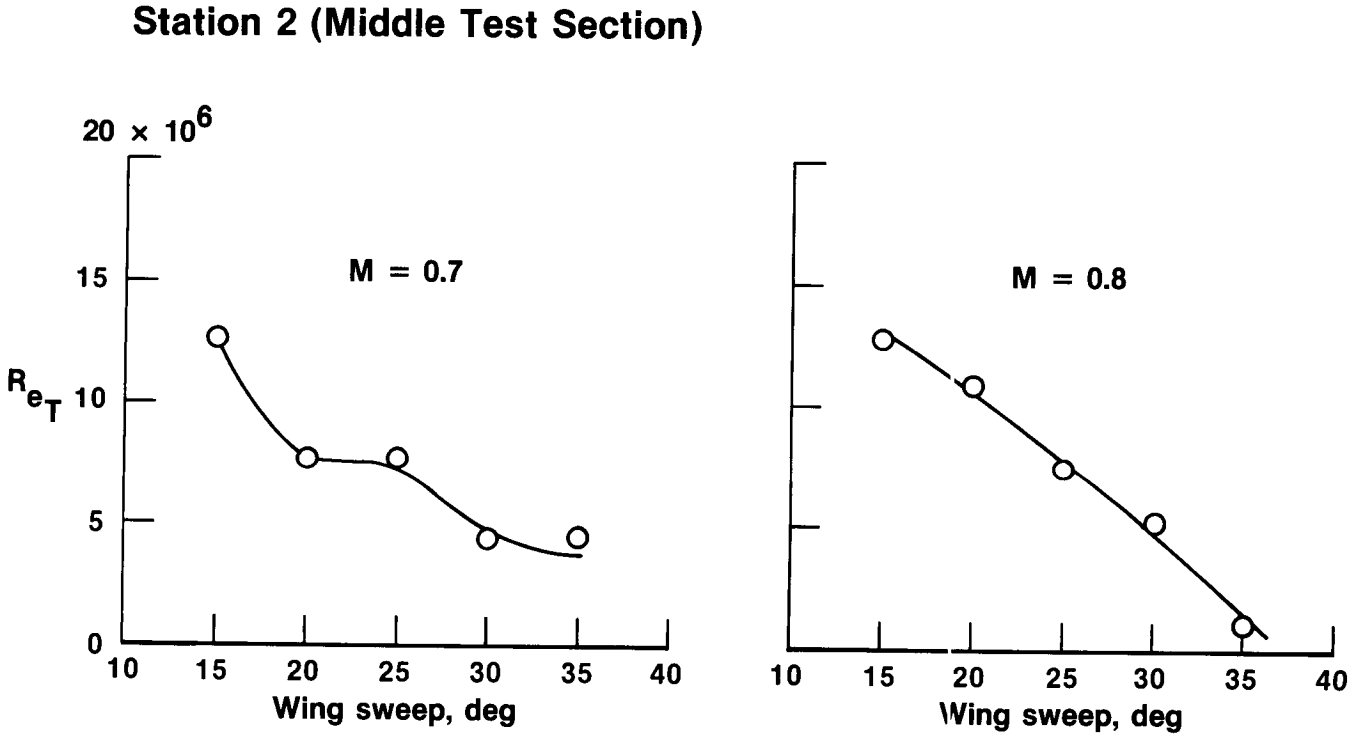

Figure 18

VISCOUS DRAG REDUCTION

Another interesting parameter available from the boundary-layer profile measurements is momentum thickness, which is an indicator of the viscous losses in the boundary layer. Figure 19 presents momentum thickness θ as a function of transition location at Mach 0.7 and a wing sweep of 20°. These data were obtained during boundary-layer rake calibration by forcing transition at known locations (see discussion of fig. 12). Maximum reductions in viscous losses were obtained at the higher altitudes (35,000 ft), as might be expected. For the outboard test section, θ varies from 0.033 at a transition location of 45-percent chord to 0.078 at a transition location of 10-percent chord. This change in θ results in a 58-percent reduction in viscous drag on the first 55-percent chord of the upper surface. Two qualifying statements apply to this viscous drag reduction: First, this experiment was not intended to be a complete airfoil test; that is, only the forward 60-percent portion of the upper wing surface is gloved, and these results indicate an optimum reduction on the upper surface of only one test section. Second, these results were not attained at working lift coefficients; that is, the pushover maneuver was required to attain the conditions that would provide extensive laminar flow. However, there is no reason to expect that an airfoil contoured specifically for high-altitude lift coefficients could not attain comparable amounts of laminar flow at working, or cruise, lift coefficents.

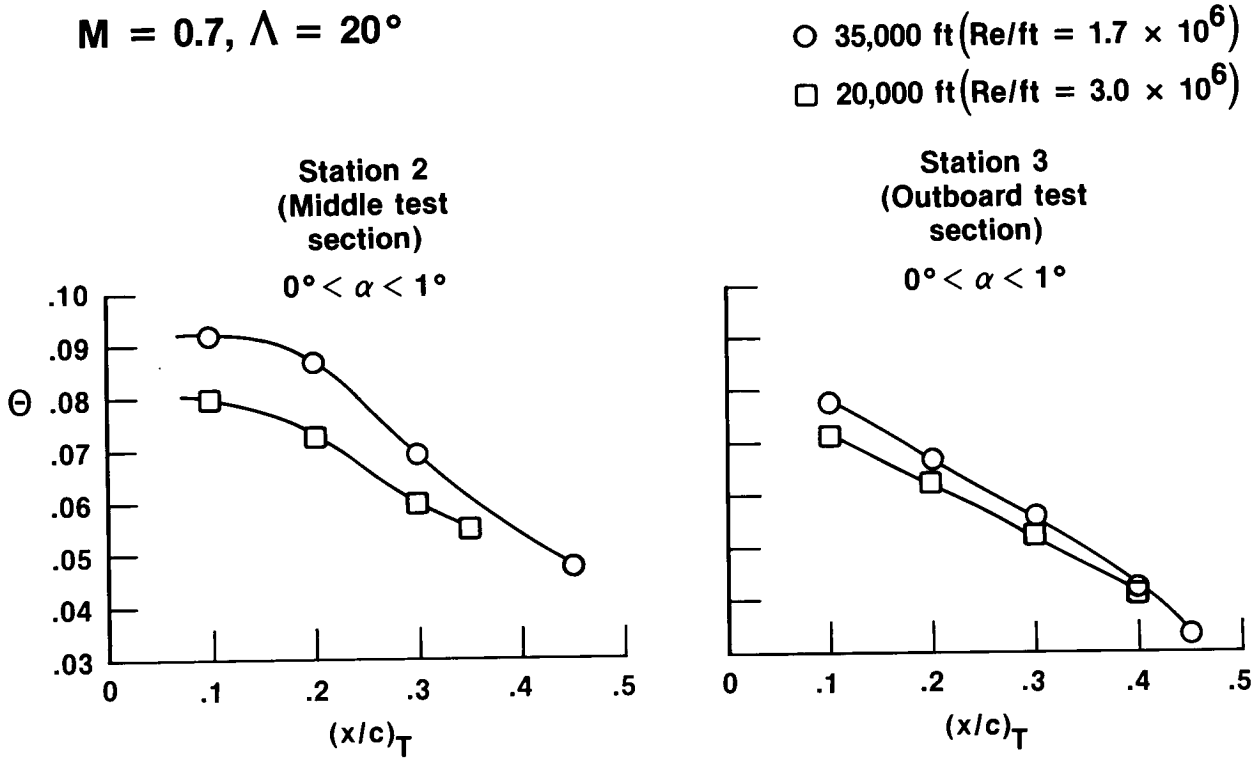

Figure 19

TYPICAL CASES FOR DETAILED ANALYSIS

During the course of the glove I flight tests, interesting results often occurred. An example is shown in figure 20, which presents three pressure distributions for a wing sweep of 30°, along with transition locations obtained from hot-film anemometer data. It is interesting to note the significant change in transition location as a result of small changes in angle of attack. For example, at an angle of attack of 0.8°, transition is between 20- and 30-percent chord; a change of approximately 1.5°, to an angle of attack of 2.3°, moves transition aft to between 40- and 50-percent chord. This change in transition location is attributed to the change in the leading edge pressure gradient, as shown in figure 20. The change in leading edge pressure gradient most likely changes the amplification of cross-flow disturbances.

Nineteen of these interesting cases, including those discussed here, have been selected and made available for detailed analysis. These cases will be discussed in detail in another paper from this conference (ref. 6).

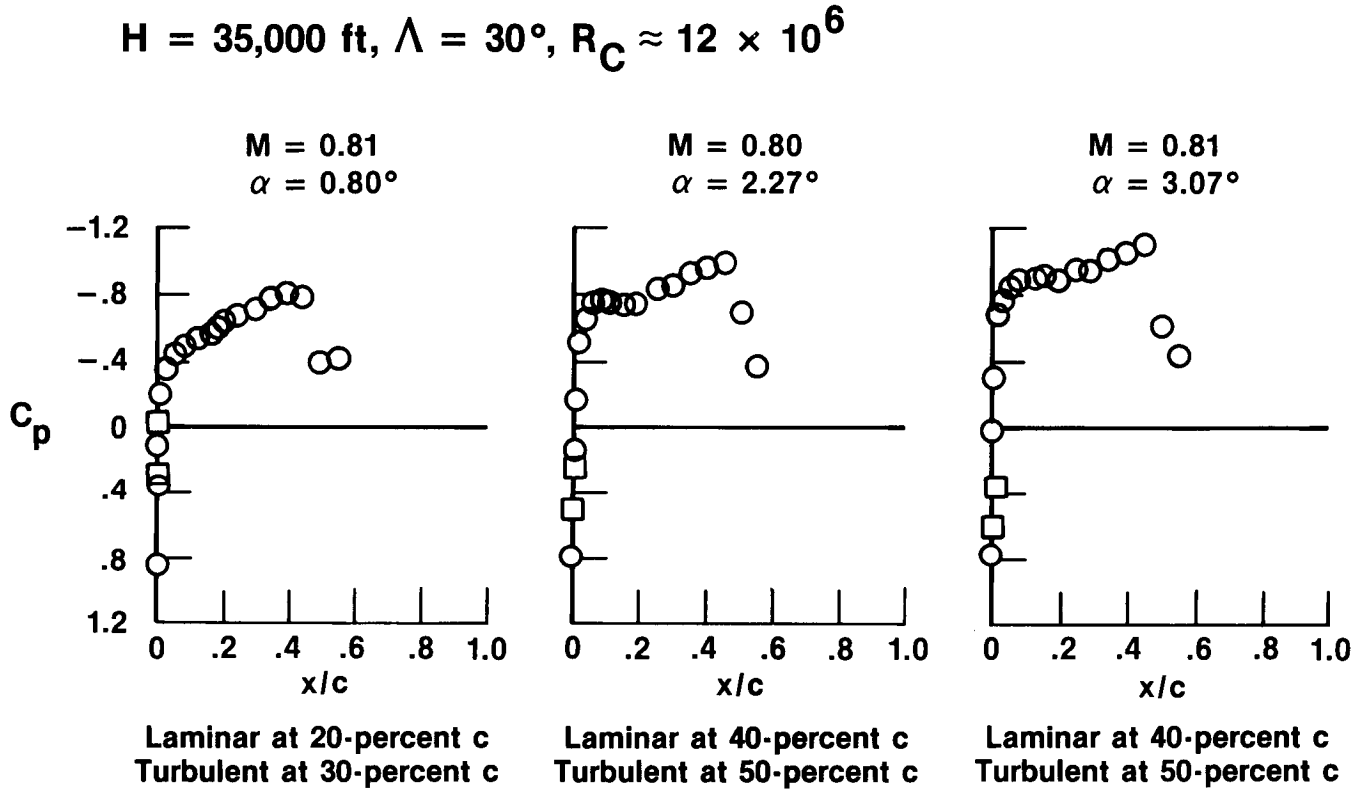

Figure 20

Concluding Remarks

- Majority of Glove 1 (cleanup) flight test have been completed
- VSTFE construction, instrumentation, and test techniques have been established
- Transition location from various methods correlate
- Preliminary results indicate a maximum transition Reynolds number of approximately 13×10^6 at 15° sweep and 5×10^6 at 35° sweep
- 19 cases selected for detailed analysis
- F-14 and associated real-time capability have proved to be a valuable laminar flow research facility
- Glove 2 will be tested

REFERENCES

1. Waggoner, E.; Campbell, R.; Philips, P.; and Hallissy, J.: Design and Tests of an NLF Wing Glove for the Variable Sweep Transition Flight Experiment. NASA CP 2487, pp. 753-776. NLF and LFC Research Symposium, Langley Research Center, Hampton, Virginia, Mar. 16-19, 1987.

2. Rozendaal, Rodger A.: Variable Sweep Transition Flight Experiment (VSTFE) - Parametric Pressure Distribution Boundary Layer Stability Study and Wing Glove Design Task. NASA CR-3992, 1986.

3. Runyan, L. James; Navran, Brent H.; and Rozendaal, Rodger A.: F-111 Natural Laminar Flow Glove Flight Test Data Analysis and Boundary Layer Stability Analysis. NASA CR-166051, 1984.

4. Meyer, Robert R., Jr.; and Jennett, Lisa A.: In-Flight Surface Oil-Flow Photographs With Comparisons to Pressure Distribution and Boundary-Layer Data. NASA TP-2395, 1985.

5. Bohn-Meyer, M.; and Jiran, Fred: The Use of Techniques to Modify Airfoils and Fairings on Aircraft Using Foam and Fiberglass. AIAA-81-2445, Nov. 1981.

6. Rozendaal, R.: VSTFE - Stability Code Development and Clean-Up Glove Data Analysis. NASA CP 2487, pp. 845-859. NLF and LFC Research Symposium, Langley Research Center, Hampton, Virginia, Mar. 16-19, 1987.

7. Mack, L.M.: On the Stability of Boundary Layer on a Transonic Swept Wing. AIAA-79-0264, Jan. 1979.

8. Hybrid Laminar Flow Control Study, Final Technical Report. NASA CR-165930, 1982.

9. Hefner, Jerry N.; and Bushnell, Dennis M.: Status of Linear Boundary Layer Stability Theory and the e^n Method, With Emphasis on Swept-Wing Applications. NASA TP-1645, 1980.

10. Malik, M.R.; and Poll, D.I.A.: Effect of Curvature on Three-Dimensional Boundary-Layer Stability. AIAA J., vol. 23, no. 9, 1985, p. 1362.

11. Malik, Mujeeb R.; Wilkinson, Stephen P.; and Orszag, Steven A.: Instability and Transition in Rotating Disk Flow. AIAA J., vol. 19, no. 9, Sept. 1981, p. 1131

12. Moes, Timothy R.; and Meyer, Robert R., Jr.: In-Flight Wing Pressure Distributions for the F-14A Aircraft. NASA TM-85921, 1985.

13. Richardson, Norman R.; and Pearson, Albin O.: Wind-Tunnel Calibrations of a Combined Pitot-Static Tube, Vane-Type Flow-Direction Transmitter, and Stagnation-Temperature Element at Mach Numbers From 0.60 to 2.87. NASA TN D-122, 1959.

14. Meyer, R.R., Jr.; and Schneider, Cdr. E.T.: Real-Time Pilot Guidance System for Improved Flight Test Maneuvers. AIAA-83-2747, Nov. 1983.

15. DeAnda, Albert G.: AFFTC Standard Airspeed Calibration Procedures. Air Force Flight Test Center. AFFTC-TIH-81-5, June 1981.

16. Johnson, J. Blair; Larson, Terry J.; and Ficke, Jules M.: Digital Program for Calculating Static Pressure Position Error. NASA TM-86726, 1987.

17. Braslow, Albert L.; and Knox, Eugene C.: Simplified Method for Determination of Critical Height of Distributed Roughness Particles for Boundary-Layer Transition at Mach Numbers From 0 to 5. NACA TN-4363, 1958.

18. Gall, P.D.; and Holmes, B.J.: Liquid Crystals for High-Altitude In-Flight Boundary Layer Flow Visualization. AIAA-86-2592, Oct. 1986.